1/20

MECHANISTIC REFLUX MODELS

Prepared for

Nuclear Regulatory Commission
Contract NRC-02-97-009

Prepared by

Stuart A. Stothoff
Goodluck I. Ofoegbu
Franklin T. Dodge
Ronald T. Green

Center for Nuclear Waste Regulatory Analyses
San Antonio, Texas

August 1998

2/20

ACKNOWLEDGMENTS

This report was prepared to document work performed by the Center for Nuclear Waste Regulatory Analyses (CNWRA) for the Nuclear Regulatory Commission (NRC) under Contract No. NRC-02-97-009. The activities reported here were performed on behalf of the NRC Office of Nuclear Material Safety and Safeguards, Division of Waste Management. The report is an independent product of the CNWRA and does not necessarily reflect the views or regulatory position of the NRC. The authors gratefully acknowledge the technical review of Debra L. Hughson, the programmatic review of William M. Murphy, and the editorial review of Barbara Long. Appreciation is due to Janet Wike and Arturo Ramos for their assistance in the preparation of this report.

QUALITY OF DATA, ANALYSES, AND CODE DEVELOPMENT

DATA: CNWRA-generated original data contained in this report meet quality assurance requirements described in the CNWRA Quality Assurance Manual. Sources for other data should be consulted for determining the level of quality for those data.

ANALYSES AND CODES: The commercial finite element code ABAQUS (Version 5.6) that was used for analysis presented in this report is controlled under CNWRA Technical Operating Procedure TOP-018, "Development and Control of Scientific and Engineering Software."

3/20

CONTENTS

4/20

FIGURES

5/20

TABLES

6/20

1 BACKGROUND AND REGULATORY CONCERNS

Corrosion rates of waste packages (WPs) emplaced at the Yucca Mountain (YM) repository may be affected by liquid water and water vapor contacting the WPs during the period of elevated temperatures caused by heat from radioactive decay after emplacement. Water dripping onto heater elements was observed in heater tests performed in fractured rock (Patrick, 1986; Ramirez, 1991). As no dripping occurred prior to the start of the testing, salt deposits can only form if thermally mobilized water drips onto the heater and subsequently evaporates. Salt deposits and high moisture availability, in conjunction with elevated temperatures, are conducive to corrosion, forming an area of potential concern for the Nuclear Regulatory Commission (NRC).

Of particular concern to the NRC are the durations and magnitudes of dripping onto the WPs during and subsequent to the thermal pulse. If thermally mobilized water only drips for a short period at the beginning of the thermal pulse, or if only a small amount of water contacts the WPs, the impact on corrosion should be relatively minor. On the other hand, if the duration and magnitude of dripping is significant or high relative humidities (RH) occur for extended periods of time during elevated temperatures, the impacts on corrosion may be significant.

Environmental factors affecting corrosion include temperature, RH, liquid moisture availability, and salt concentrations. The U.S. Department of Energy is performing heater tests in the Topopah Spring welded unit (Buscheck and Nitao, 1995; Buscheck et al., 1993) to examine possible drift-scale responses of these factors during a relatively short and intense test. Despite the utility of this *in situ* testing, the heater tests cannot identify the long-term behavior (e.g., over hundreds of years) of the rock mass due to temporal and spatial limitations. Numerical approaches provide feasible methods for bounding the behavior of the environmental factors over such long periods of time.

The NRC has adopted a screening approach to investigate the impacts on the WPs of the moisture in the rock mass surrounding each drift. The primary concern is to quantify potential durations and magnitudes of dripping onto the WPs. If dripping occurs only during extremely restricted periods or with extremely restricted magnitudes, it will not be necessary to consider the salt concentrations in great detail. Only the temperature and RH values are of interest for corrosion and moisture regimes may be acceptably handled during the thermal pulse in Total-System Performance Assessment exercises, in simple ways. On the other hand, if it can be shown that extensive dripping may occur under plausible hydrothermal conditions, the impact of dripping on corrosion may not be neglected without further analysis, warranting a more-detailed investigation.

Refluxing is the primary mechanism considered by the NRC[1] that would promote dripping onto WPs under boiling conditions. The energy in latent heat cools the rock mass upon boiling and is released when the steam condenses. The effect is to form a heat pipe, in which an extensive mass of rock is at or near the boiling temperature. The liquid water primarily is driven by capillary and gravity effects, while the steam moves primarily due to gas-phase pressured differences due to addition of vapor from boiling, so that a heat pipe may form both above and below the repository. The localized water movement may significantly cool the fracture carrying the heat pipe relative to the surrounding rock mass. If this local movement is not handled

[1]Input to Issue Resolution Status Report: Key Technical Issue: Thermal Effects on Flow, 1998, Predecisional document submitted to Nuclear Regulatory Commission.

appropriately in the modeling process, neglect of the local cooling would not allow penetration of the water further into the boiling zone (hence, closer to the drift) than would be otherwise predicted.

As current methods for considering refluxing have significant limitations, there is a great deal of uncertainty in the expected behavior at YM. The interaction of refluxing with individual drifts is at an awkward scale, with too few fractures per unit volume to use continuum methods with great confidence and too many fractures per unit volume to discretize discrete fractures using standard computational methods.

This status report presents steps toward developing an alternative approach to discrete-fracture simulations of refluxing. The alternative approach uses boundary integral methods to dispense with the requirements of discretizing the matrix, so that computational effort is concentrated on the physics in and near discrete fractures. The use of boundary integral methods allows for the behavior to be examined anywhere within the repository (e.g., at the edge or at the center) without significant difficulties. The general methodology allows for the boiling isotherm to be tracked within the matrix, as a sharp interface between vapor and liquid, using the approximation that the system is in a quasi-steady state. The methodology is developed in section 2. Note that refinement of the methodology is expected as experience builds and coding progresses.

The methodology has not been fully coded or tested; however, a cross-comparison between the new boundary integral code (used to assess the viability of the approach) and ABAQUS (a standard finite element simulator) shows excellent agreement for a special case developed to examine the potential of the methodology for these types of problems, before going to the effort of coding the general case. The special case is a thermal-only problem, a single fracture in a rock matrix, with water introduced at the top of the fracture at various rates. The water is not explicitly modeled, but the energy transfer due to boiling is qualitatively handled by using sources and sinks with a magnitude equal to the latent heat necessary to boil the given amount of infiltrating water. The problem is similar to the case where impermeable fracture coatings exist. The idea of the special case is to evaluate quasi-steady-state refluxing at various levels of repository heating. The test problem and comparison are discussed in section 3.

The special case is convenient for comparisons of the new methodology with existing methods. In addition, the special case is amenable to analysis with standard finite element methods, yielding qualitative information on the effect of infiltration rates and source strength on refluxing and drift temperatures. A demonstration analysis, using a finite element approach, is presented in section 3.2, where it is suggested that infiltration rates commonly used for performance assessment (e.g., 5–10 mm/yr) focused over a reasonable area (e.g., 100 m^2/m) into a single fracture, may lower the drift temperature sufficiently to permit dripping. The analysis neglects vapor transport past the drift, however, which may be an effective alternative mechanism for allowing the infiltrating water to pass through the repository horizon.

2 COMPUTATIONAL APPROACH

2.1 BACKGROUND

A variety of computational approaches has been used to quantify moisture redistribution due to the thermal pulse, ranging from the mountain scale to the single-fracture scale. Most approaches try to treat the fracture-matrix system as continua, enabling a tremendous reduction of the computational problem (discrete fractures are not considered) in return for fracture-matrix exchange terms that are generally poorly identified. Approaches that YM investigators have adopted include (i) single continuum (either fracture-only or matrix-only); (ii) equivalent-continuum (the matrix and fractures are assumed to be in equilibrium so that the exchange between matrix and fractures is not explicitly considered); (iii) dual-continuum (the matrix and fractures are linked with some exchange term accounting for the spacing of active fractures); and (iv) multiple-continuum (the dual-continuum matrix blocks are conceptually subdivided).

Semi analytic approaches offer possible insight into the mechanism active within a discrete fracture. Ongoing work at the Center for Nuclear Waste Regulatory Analyses (CNWRA) has attempted to investigate refluxing behavior in a single discrete fracture using the finite volume method, a standard numerical approach that is the basis for the TOUGH family of codes and MULTIFLO (Lichtner and Seth, 1998). The advantage of the finite volume approach is in generality, where the physics of the problem can be described readily and many problem geometries can be discretized. Investigation has shown that when attacking a discrete-fracture problem, particularly with strong thermal excitations, the finite volume approach is extremely demanding computationally. The fracture and matrix react at vastly different spatial and temporal scales and the small space and time scales required for properly discretizing the fractures impose a great computational burden when extended to the matrix scale. The resulting computational burden limits finite volume computations to unrealistically small problems.

The computational burden imposed by standard domain methods (e.g., the finite volume method) led CNWRA researchers to seek alternate approaches for handling the matrix/fracture interactions. Boundary integral methods are known to be attractive with domain approaches for certain types of problems. The methods are most competitive for steady-state diffusion problems with constant coefficients, such as heat conduction in a uniform rock matrix. Boundary integral methods have also been successfully used for tracking free surfaces, such as phase-change boundaries and phreatic water tables. The physical problem can be cast into a form that takes advantage of these strengths, by recognizing that the system is often in a quasi-steady state amenable to the boundary integral approach.

One advantage of the boundary integral approach is that the computational mesh is only defined at the boundary and on internal discontinuities, thereby greatly reducing the number of unknowns during the solution process. Internal discontinuities include formation boundaries, fractures, and phase change boundaries. The solution is analytic away from discontinuities and boundaries. One of the strengths of the boundary integral approach is that the entire mountain can be accounted for with little additional computational burden when considering behavior in a single fracture. Further, the discretization for a single fracture is reduced in dimensionality from that of domain methods such as the finite volume method. For example, fractures are one-dimensional features in two-dimensional (2D) problems, rather than 2D features; in three-dimensional (3D) problems, fractures are 2D surfaces.

An overall approach for considering quasi-steady state coupled heat and moisture transport in an unsaturated fractured rock matrix is developed in this section. It is assumed that a few fractures will be discretized explicitly, with detailed transport calculations occurring within these fractures. Other fractures may also be included but not explicitly discretized, using the equivalent-continuum assumption. It is assumed that the primary interest is in capturing conditions in and near the discrete fractures. Accordingly, the response of the rock matrix far from the discrete features is captured more approximately than the explicit response between the discrete fractures and the rock matrix near the fractures.

2.2 DESCRIPTION OF BOUNDARY INTEGRAL EQUATION METHOD

The Green's function, or direct boundary element approach, is followed herein due to the generality of the approach and the ease of incorporating extensions to the basic formulation. An excellent derivation of the approach is presented by Liggett and Liu (1983), along with the associated computer code. Summary discussions of the methodology are presented by Stothoff (1991). Presentation of the method assumes there is one potential of interest, such as temperature, for clarity. Actual application of the method may use several coupled equations in several unknowns. Development of the approach is for a steady-state system, although in general time-dependent cases may also be considered.

The Green's function approach takes advantage of Green's theorem. The first form of Green's theorem states that, for a function V satisfying the divergence theorem (in 1, 2, or 3 spatial dimensions)

$$\int_{\Omega} \nabla \cdot \boldsymbol{V} \, d\Omega = \int_{\sigma} \boldsymbol{n} \cdot \boldsymbol{V} \, d\sigma \tag{2-1}$$

where ∇ is the gradient operator, Ω is the domain of interest, σ is the domain boundary, $\boldsymbol{n}$ is the vector normal to the boundary, V is represented by $V = \phi \nabla G$, and both ϕ and G are scalar functions of space,

$$\int_{\Omega} \nabla \cdot \phi \nabla \boldsymbol{G} \, d\Omega = \int_{\sigma} \boldsymbol{n} \cdot \phi \nabla \boldsymbol{G} \, d\sigma \tag{2-2}$$

A symmetric form of Eq. (2-2) is derived by applying the first form of the Green's theorem to the second part of the left hand side, reversing the role of ϕ and G, resulting in the second form of the Green's theorem

$$\int_{\Omega} \left(\phi \, \nabla^2 \boldsymbol{G} - \boldsymbol{G} \, \nabla^2 \phi \right) d\Omega = \int_{\sigma} \boldsymbol{n} \cdot \left(\phi \, \nabla \boldsymbol{G} - \boldsymbol{G} \nabla \phi \right) d\sigma \tag{2-3}$$

If an appropriate function G is found which satisfies the relationship

$$\nabla^2 \boldsymbol{G} = \delta \left(\boldsymbol{p} - \boldsymbol{d} \right) \tag{2-4}$$

then,

$$\int_{\Omega} \phi \nabla^2 G d\Omega = \alpha \phi(p) \tag{2-5}$$

The second part of the volume integral in Eq. (2-3) is identically zero, resulting in

$$\alpha \phi(p) = \int_{\sigma} \left(\phi(d) \frac{\partial G}{\partial n}(p,d) - G(p,d) \frac{\partial \phi}{\partial n}(d) \right) d\sigma \tag{2-6}$$

where the notation $\partial\phi/\partial n$ is shorthand for the expression $n \cdot \nabla \phi$. This is the basic representation for the direct boundary integral method used herein. With this representation, ϕ may be found at any base point p by setting the field point d to the locus of points defining the surface. For the free space Laplace equation in 2D,

$$G = \frac{\ln(r)}{2\pi} \tag{2-7}$$

and for the free space Laplace equation in 3D,

$$G = \frac{1}{4\pi r}, \tag{2-8}$$

where $r = |p-d|$. The coefficient α depends on the location of the point p relative to the jump in potential along σ as it arises from the exclusion of the singular point $p = d$ from Ω; α is zero if p is outside Ω, 1 if p is wholly within Ω, and 1/2 if on a smooth portion of the boundary.

If p lies at a nonsmooth portion of the boundary, α corresponds to the interior angle the boundary makes at the point. Note that $\partial\phi/\partial n$ does not have a unique value at points where the boundary is not smooth, as there is no well-defined normal direction. This difficulty is handled by defining $\partial\phi/\partial n$ by pieces, with discontinuities occurring at angle points.

Equation (2-6) expresses the value of potential at a point as a sum of a weighted integral of the potential around σ and a weighted integral of the normal derivative of the potential around σ. If both of these values are known, in theory the potential may be found at any internal or boundary point. Liggett and Liu (1983) report that solutions tend to deteriorate near σ, due to what is termed the boundary layer effect. This arises due to the sharp change in α at σ. Care must be taken to minimize this numerical artifact.

In a well-posed problem, either ϕ or $\partial\phi / \partial n$ is defined around σ. For boundary integral methods to work, the missing boundary values must be available; to generate the missing set of boundary values, a number of strategies are commonly used. In the most common approach, both ϕ and $\partial\phi / \partial n$ are discretized into point values and interpolating functions between the point values, with a resultant set of N unknown values. Equation (2-6) is applied directly at the N locations where an unknown value is desired, resulting in a complete set of N equations in N unknowns. This is denoted by the matrix equation

$$H\,\phi = G\frac{\partial\phi}{\partial n} \tag{2-9}$$

where H comprises the integrals, dependent on the geometry of the problem, which multiply the discretized point values of ϕ, and G comprises the corresponding integrals for the point values of $\partial\phi / \partial n$. In practice, this equation is rearranged so that known values are multiplied through and placed on the right hand side and unknown values are moved to the left hand side, resulting in the familiar system of equations

$$Au = b \tag{2-10}$$

where A is a square matrix, u is the vector of unknown, ϕ and $\partial\phi / \partial n$ values, and b is a vector of known information.

If the Green's function is satisfied identically along a portion of σ, the corresponding portion of σ need not be discretized; for example, a Green's function can be constructed that explicitly takes into account no-flow conditions on a boundary, using the method of images. The free space Green's function accommodates infinite boundaries and only *finite* boundaries need be discretized. This property is in stark contrast to domain method requirements.

Another approach uses the derivative of Eq. (2-6) to evaluate the normal derivative at the boundary directly. The derivative of ϕ in an arbitrary direction n_p may be written in the form

$$\alpha\frac{\partial\phi}{\partial n_p}(p) = \frac{\partial}{\partial n_p}\left[\int_\sigma\left(\phi(d)\,\frac{\partial G}{\partial n}(p,d) - G(p,d)\,\frac{\partial\phi}{\partial n}(d)\right)\,d\sigma\right] \tag{2-11}$$

Equation (2-11) may be evaluated at any point for which Eq. (2-6) is valid, with a caveat for a base point p on σ. When the base point is not on the boundary, the derivative of the integrals may be taken inside the integral, resulting in

$$\alpha\frac{\partial\phi}{\partial n_p}(p) = \int_\sigma\left(\phi(d)\,\frac{\partial^2 G}{\partial n_p \partial n}(p,d) - \frac{\partial G}{\partial n_p}(p,d)\,\frac{\partial\phi}{\partial n}(d)\right)\,d\sigma \tag{2-12}$$

On the other hand, when the base point is on σ, the singularities resulting from coincidence of the base point p and the field point d in Eq. (2-12) are too strong to be integrated directly. As is shown by Ingber and Mitra (1989), the resulting integral may be evaluated in the finite-part sense, or Eq. (2-11) may be evaluated by taking the derivative *after* performing the integration. In either case, both the boundary and the normal gradients must be smoothly varying at the point of evaluation to perform the requisite operations. This precludes the use of Eq. (2-11) at either angle points or jumps in normal gradient values. The more straightforward approach to evaluate Eq. (2-11) is to take the derivative of the integral rather than evaluate the integral in the finite-part sense.

Experience suggests that simple approaches produce quite acceptable results. Piecewise linear ϕ and piecewise constant $\partial\phi / \partial n$, together with adequate numbers of elements, are quite sufficient to avoid most difficulties. In fact, piecewise constant ϕ is adequate for most cases.

2.3 INCORPORATION OF INTERNAL DISCONTINUITIES

The general boundary integral formulation for flow in the matrix provides values for u or $\partial u / \partial n$ at particular points on the boundary or within the domain of interest, where u is the potential of interest. The formulation is

$$\begin{aligned} \sum_i \alpha_i u_i &= \int_\sigma \left(G \frac{\partial u}{\partial n} - u \frac{\partial G}{\partial n} \right) d\sigma + \int_{\sigma_M} \left(G \Delta \frac{\partial u}{\partial n} - \Delta u \frac{\partial G}{\partial n} \right) d\sigma_M, \\ &= \int_\sigma \left(G \frac{\partial u}{\partial n} - u \frac{\partial G}{\partial n} \right) d\sigma + \int_{\sigma_M} \left(-G q_s - \Delta u \frac{\partial G}{\partial n} \right) d\sigma_M, \end{aligned} \tag{2-13}$$

where G is the Green's function, q_s is the flux entering the fracture, Δ is the jump operator (e.g., $\Delta u = u_1 - u_2$, where the subscripts represent sides 1 and 2 of the discontinuity), σ represents the domain boundary, σ_M represents discontinuities within the domain, and α_i is the fraction of the point in region i (the point may be partially within several domains). If the point is completely within the domain, $\alpha = 1$. On a smooth boundary, $\alpha = 1/2$.

The boundary integral method requires that all terms within the integrals are known before ϕ can be explicitly evaluated at any point. A well-specified problem does not provide all terms. To define the missing terms, a set of linear equations is formed by writing one equation for each unknown. Choosing the representation of piecewise-linear u and piecewise-constant $\partial u / \partial n$, equations along the boundary are written at nodes wherever there is an unspecified value of u and are written at element centroids wherever there is an unspecified value of $\partial u / \partial n$. The jump values may be known or unknown, but generally arise from the application of compatibility equations for continuity of the unknown or the gradient of the unknown. If unknown, the jump values must also be determined during the solution process.

In the following, the basic unknown of interest is potential (ϕ), where ϕ might represent temperature or pressure. Where piecewise constant matrix properties exist, u may represent $K_m \phi$, where K_m represents matrix conductivity, thereby simplifying notation without loss of generality. Accounting for the matrix

conductivity, flux at a point in the matrix is represented by $q = -K_m \nabla \phi = -\nabla u$. In fractures it may be more convenient to use ϕ directly, as the physical processes are more complex.

Along discontinuities, compatibility between and flux must be achieved, but there are numerous possible conditions. Through-flux from matrix to matrix across the fracture may be limited by increased resistance within the fracture and the matrix blocks may have different conductivities. The number of cases can be collapsed into a general case of flow passing normal to the fracture, which can then be specialized as necessary. The fracture represents a resistance to flow, with several causes, that can be grouped into a single resistance (or conductance). Fracture conductances (conductivity, K, divided by thickness b) are consistently formed by considering the case where three distinct (and isotropic) layers form the fracture. In sequence, the layers might represent a fracture coating (subscript 1), fluid (subscript 2), and another fracture coating (subscript 3). The total conductance for flow normal to the fracture is then

$$C_{norm} = \frac{\theta}{\sum_{i=1}^{3} \frac{b_i}{K_i}} + \frac{(1-\theta)K_{bypass}}{\sum_{i=1}^{3} b_i} \tag{2-14}$$

while the total conductance for flow over a distance L along the fracture is

$$C_{tang} = \frac{\sum_{i=1}^{3} b_i K_i}{L \sum_{i=1}^{3} b_i} \tag{2-15}$$

The fraction of the surface area of the fracture contributing to fracture/matrix exchange is denoted by θ; the remainder is assumed to contribute to fracture-bypass fluxes (e.g., through matrix-to-matrix contact along asperities) with conductivity K_{bypass}. The consistent representation for conductances becomes

$$C_{e1} = \frac{\theta}{\frac{b_1}{K_1} + \frac{b_2}{(2K_2)}} \tag{2-16}$$

$$C_{e2} = \frac{\theta}{\frac{b_3}{K_3} + \frac{b_2}{(2K_2)}} \tag{2-17}$$

$$\overline{C} = \frac{1}{2}\left(C_{e1} + C_{e2}\right) \tag{2-18}$$

$$\Delta C = C_{e2} - C_{e1} \tag{2-19}$$

These representations are consistent even if the fracture coatings do not exist ($b_1 = 0$ .and/or $b_3 = 0$).

A boundary integral equation for any material-derived discontinuity can be written at the element centroids: (i) values for ϕ at the surrounding nodes or the centroid, (ii) jumps in u at the centroid, (iii) integrals of the normal equation, and (iv) integrals of the derivative equation. In the most complex cases, both Eqs.(2-20) and (2-21) are required; otherwise , one equation is. The full equations are

$$\begin{aligned} a_{11}q_s + a_{12}\Delta u = f_{11}&\left[\int_{\sigma}\left(G\frac{\partial u}{\partial n} - u\frac{\partial G}{\partial n}\right)\,d\sigma + \int_{\sigma_M}\left(-Gq_s - \Delta u\,\frac{\partial G}{\partial n}\right)\,d\sigma_M\right] \\ + f_{12}\frac{\partial}{\partial n}&\left[\int_{\sigma}\left(G\frac{\partial u}{\partial n} - u\frac{\partial G}{\partial n}\right)\,d\sigma + \int_{\sigma_M}\left(-Gq_s - \Delta u\,\frac{\partial G}{\partial n}\right)\,d\sigma_M\right] \end{aligned} \tag{2-20}$$

$$a_{21}q_s + a_{22}\Delta u + a_{23}\phi = f_{21}\left[\int_{\sigma}\left(G\frac{\partial u}{\partial n} - u\frac{\partial G}{\partial n}\right)\,d\sigma + \int_{\sigma_M}\left(-Gq_s - \Delta u\frac{\partial G}{\partial n}\right)\,d\sigma_M\right] \tag{2-21}$$

where

$$a_{11} = -1 \tag{2-22}$$

$$a_{12} = \frac{C_{norm}}{2}\left(\frac{1}{K_{m2}} + \frac{1}{K_{m1}}\right) \tag{2-23}$$

$$f_{11} = - C_{norm} \left(\frac{1}{K_{m2}} - \frac{1}{K_{m1}} \right) \tag{2-24}$$

$$f_{12} = 1 \tag{2-25}$$

$$a_{21} = - 1 \tag{2-26}$$

$$a_{22} = - \frac{\overline{C}}{2} \left(\frac{1}{K_{m2}} - \frac{1}{K_{m1}} \right) - \frac{\Delta C}{4} \left(\frac{1}{K_{m2}} + \frac{1}{K_{m1}} \right) \tag{2-27}$$

$$a_{23} = 2\overline{C} \tag{2-28}$$

$$f_{21} = \overline{C} \left(\frac{1}{K_{m2}} + \frac{1}{K_{m1}} \right) + \frac{\Delta C}{2} \left(\frac{1}{k_{m2}} - \frac{1}{K_{m1}} \right) \tag{2-29}$$

where K_{m1} and K_{m2} represent the matrix conductivities on either side of the fracture. Eq. (2-20) can be referred to as the Δh equation while Eq. (2-21) can be referred to as the Δg equation.

A fracture mass balance equation for each fracture element explicitly accounts for diffusion between adjacent nodes, transfer between the matrix and fracture, and sources and sinks within the fracture. The sources and sinks might be externally applied (e.g., for testing purposes), but can also be used to capture advection and phase change effects. The fracture mass balance equation for fracture node i is

$$\sum_j C_{tang\,ij} \left(\phi_j - \phi_i \right) + \sum_k A_{nfk} q_{sk} + Q_{ci} = 0, \tag{2-30}$$

where A_{nfk} is the area of the fracture exchanging with the matrix associated with the node ($A_{nfk} = L_k/2$ in 2D), the summation over j represents the number of nodal connections exchanging with node i, the summation over k represents the number of elements attached to node i, and Q_{ci} represents internal sources and sinks.

2.4 GOVERNING EQUATIONS

The governing equation for mass transport in a porous medium is, written, in terms of a species i in a phase α

$$\frac{\partial}{\partial t}\left(\epsilon_\alpha \rho_\alpha \omega_\alpha^i\right) + \nabla \cdot \left(\epsilon_\alpha \rho_\alpha \omega_\alpha^i \boldsymbol{v}_\alpha\right) + \nabla \cdot \boldsymbol{j}_\alpha^i = \boldsymbol{S}_\alpha^i \qquad (2\text{-}31)$$

where ϵ_α is the volume fraction of phase α ($\epsilon_\alpha = \epsilon\, \theta_\alpha$, where ϵ is porosity and θ_α is the saturation of phase α), ρ_α is the density of phase α, ω_α^i is the mass fraction of species i in phase α, v_α is the mass average velocity of phase α, j_α^i is the nonadvective flux of species i in phase α, and S_α^i is the exchange of mass of species i into phase α due to interphase interaction (e.g., boiling).

In addition to an equation for each species i in each phase α, the following constraints follow from the definition of volume average and mass average:

$$\sum_{i=1}^{N_{spec}} \omega_\alpha^i = 1 \qquad (2\text{-}32)$$

$$\sum_{\alpha=1}^{N_{phase}} \epsilon_\alpha = 1 \qquad (2\text{-}33)$$

In addition, when interfaces between phases are massless,

$$\sum_{\alpha=1}^{N_{phase}} \boldsymbol{S}_\alpha^i = 0 \qquad (2\text{-}34)$$

For problems of interest at YM, the number of species (N_{spec}) is 2 (water and air) and the number of phases (N_{phase}) is 3 (liquid, gas, and solid). The solid phase is assumed to be immobile and does not exchange mass, so that an equation for the solid phase is not required.

Darcy's Law provides a relationship between the velocity of a fluid phase relative to a porous medium, the gradient of the fluid pressure, and the acceleration due to gravity. A multiphase analogy to Darcy's Law, assuming an immobile solid phase, is defined by

$$\boldsymbol{v}_\alpha = -\frac{\boldsymbol{k}\boldsymbol{k}_{r\alpha}}{\boldsymbol{\mu}_\alpha \epsilon_\alpha} \cdot \left(\nabla \boldsymbol{P}_\alpha + \rho_\alpha \boldsymbol{g} \nabla \boldsymbol{z}\right) = -\frac{\boldsymbol{k}\lambda_\alpha}{\epsilon_\alpha} \cdot \left(\nabla \boldsymbol{P}_\alpha + \rho_\alpha \boldsymbol{g} \nabla \boldsymbol{z}\right) \tag{2-35}$$

where k is the intrinsic permeability of the porous medium, λ_α is the mobility of phase α $\left(\lambda_\alpha = k_{r\alpha}, \mu_\alpha\right)$, $k_{r\alpha}$ is the relative permeability of phase α $(0 \le k_{r\alpha} \le 1, \mu_\alpha)$ is the dynamic viscosity of phase α, P_α is the pressure of phase α, g is the acceleration due to gravity, and z is the elevation above a reference datum.

The nonadvective flux of binary species within a phase through diffusion and dispersion is (Bird et al., 1960)

$$\boldsymbol{j}_\alpha^i = -\boldsymbol{D}_\alpha \rho_\alpha \nabla \omega_\alpha^i = -\boldsymbol{D}_\alpha \rho_\alpha \nabla \left(\frac{\rho_\alpha^i}{\rho_\alpha}\right) \tag{2-36}$$

where D_α is a diffusion coefficient and ρ_α^i is the density of species i in phase α. The diffusion coefficient typically has the form $D_\alpha = \tau \epsilon_\alpha D$, where τ is a factor accounting for tortuous paths and D is the diffusion coefficient in phase α.

The general approach for considering a moving phase-change boundary in the rock matrix using boundary integral methods treats the boiling isotherm as a sharp interface between a gas-dominated region and a liquid-dominated region. In both regions, it is assumed that both mass transport and energy transport are at a quasi-steady state, or equilibrated rapidly relative to the movement of the sharp interface. Within the boiling region, it is assumed that moisture moves predominantly due to vapor transport, while within the subboiling region it is assumed that moisture moves predominantly in the liquid phase. All energy transfer due to boiling and condensation is assumed to occur at the sharp interface.

With these assumptions, the quasi-steady state governing equation for vapor mass balance in the boiling zone is

$$\nabla \cdot \left[\rho_v \boldsymbol{k} \lambda_g \left(\nabla \boldsymbol{P}_g + \rho_g \boldsymbol{g} \nabla \boldsymbol{z}\right)\right] + \nabla \cdot \boldsymbol{D}_g \rho_g \nabla \omega_g^v = \boldsymbol{0} \tag{2-37}$$

where P_g is gas pressure, λ_g is gas mobility, D_g is the diffusion coefficient, and ρ_v is vapor density $\left(\rho_v = \omega_g^v \rho_g\right)$. Summing the vapor equation and a similar equation for the air species yields

$$\nabla \cdot \left[\rho_g \boldsymbol{k} \lambda_g \left(\nabla \boldsymbol{P}_g + \rho_g \boldsymbol{g} \nabla \boldsymbol{z}\right)\right] = \boldsymbol{0} \tag{2-38}$$

which, using the ideal gas law ($P = \rho RT$, where R is the specific gas constant for the gas), can be rewritten

$$\nabla\left[k\lambda_g\left(R\left(\rho_g^2\nabla T + \frac{T}{2}\nabla\rho_g^2\right) + \rho_g^2 g\nabla z\right)\right] = 0 \tag{2-39}$$

The result is an equation for gas density dependent on temperature. Assuming it is acceptable to use a representative mean value for T, k, λ, and ρ, the mass governing equation can be written

$$A_1\,\nabla^2\,\rho_g^2 + A_2\,\nabla^2\,T + A_3\,\nabla^2 z = 0 \tag{2-40}$$

$$A_1 = \left\langle\frac{RTk\lambda_g}{2}\right\rangle \tag{2-41}$$

$$A_2 = \langle R\rho_g^2 k\lambda_g\rangle \tag{2-42}$$

$$A_3 = \langle\rho_g^2 k\lambda_g\rangle \tag{2-43}$$

The braces denote the representative value. The representative values might be obtained by averaging several point values strategically located within the domain after each nonlinearity iteration. The approximated governing equation is a sum of Laplacians, each of which can be written as a boundary integral.

The governing equation for energy in the boiling zone can be written

$$\nabla\,(Cq) - \nabla\cdot\left(K_e\,\nabla\,T\right) = 0 \tag{2-44}$$

$$q = -\,A_1\,\nabla\rho_g^2 - A_2\,\nabla\,T - A_3\,\nabla z \tag{2-45}$$

where C is specific enthalpy for the air mixture, q is flux of the air mixture, and K_e is thermal conductivity. When all coefficients are spatially invariant, the energy equation may be calculated as a sum of Laplacians that can be solved using boundary integrals. The governing mass balance equation and energy balance equation must be solved simultaneously.

Within the subboiling zone, the quasi-steady state governing equation for liquid flow is (assuming there is negligible air dissolved in the liquid)

$$\nabla \cdot \boldsymbol{K}\left(\nabla \boldsymbol{P}_l + \rho_l \boldsymbol{g} \nabla \boldsymbol{z}\right) = \boldsymbol{0} \tag{2-46}$$

If $K = K_{sat} \exp(\alpha P_l)$, where α is now a scaling parameter and should not be confused with an index [e.g., the Gardner approximation (Gardner, 1958)], the governing equation can be converted to

$$\nabla^2 \phi = \boldsymbol{s}^2 \phi \tag{2-47}$$

which is quasi-linear, with the following substitutions

$$\phi = \exp\left(-\boldsymbol{s}z\right) \int_{-\infty}^{P_l} \boldsymbol{K} \, d\boldsymbol{P}_l = \frac{\boldsymbol{K}_{sat}}{\alpha} \exp\left(\alpha \boldsymbol{P}_l - \boldsymbol{s}z\right) \tag{2-48}$$

$$\boldsymbol{s} = \frac{\rho \boldsymbol{g} \alpha}{\boldsymbol{2}} \tag{2-49}$$

The correspondence between fluxes is

$$\frac{\partial \boldsymbol{q}}{\partial \boldsymbol{n}} = \boldsymbol{K}\left(\boldsymbol{P}_l\right) \frac{\partial \boldsymbol{P}_l}{\partial \boldsymbol{n}} = \exp(\boldsymbol{s}z) \left[\frac{\partial \phi}{\partial \boldsymbol{n}} + \boldsymbol{s}\phi \frac{\partial \boldsymbol{z}}{\partial \boldsymbol{n}}\right] \tag{2-50}$$

The Green's function for the quasi-linear case is (Pullan and Collins, 1987)

$$G = K_0(sr) \qquad in\ 2D \tag{2-51}$$

$$G = \frac{\exp(-sr)}{r} \quad in\ 3D \tag{2-52}$$

where K_0 is the modified Bessel function of the second kind of order 0. Any effect of temperature on K and ρ are neglected. The quasi-steady state governing equation for gas mass balance in the subboiling zone is identical to the governing equation in the boiling zone. Different values for the coefficients may be required in the two zones.

The energy balance equation in the nonboiling zone is

$$\nabla \cdot (K_e \nabla T) = 0 \tag{2-53}$$

It is assumed that conduction is the only significant means of heat transport in the nonboiling zone. In the nonboiling zone, mass and energy fluxes are assumed independent. The approach in the subboiling zone features a strong assumption, in particular that vapor fluxes are negligible in the nonboiling zone even with a strong temperature gradient. This strong assumption is made as a consequence of the quasi-linear approximation for unsaturated flow, which makes it difficult to apply superposition. The impact of the approximation remains to be examined.

2.5 INTERFACE COMPATIBILITY CONDITIONS

At the isotherm, vapor pressure in the boiling zone is determined by saturated vapor pressure at the boiling temperature times the RH (considered solely as a function of the liquid pressure). Total pressure is determined from the gas phase equation, which is continuous at the isotherm.

The compatibility of pressures at the boiling isotherm is nonlinear. A reasonable approach for this nonlinearity is to assume an initial liquid pressure distribution along the isotherm and solve for the increment in pressure. The procedure uses the linearization

$$P_v^{m+1} \approx P_v^m + \frac{dP_v}{dP_l}\,\delta P_l \tag{2-54}$$

where liquid and vapor are denoted by l and v, P is pressure, m represents the iteration level, and the unknown being determined is δP_l.

The temperature at the isotherm is specified as the boiling temperature. The boiling temperature might be considered a function of pressure, represented by the sum of air pressure and vapor pressure, although this correction is small for YM.

The compatibility equations for mass and energy fluxes are coupled through the velocity of the isotherm. The velocity, V, of a discontinuity (shock) in an incompressible phase is

$$V = \frac{q_2 - q_1}{\epsilon(\theta_2 - \theta_1)} \tag{2-55}$$

where q is flux, ϵ is porosity, θ is saturation (or mass fraction times saturation, for vapor), and the subscript represents the side of the discontinuity. Note that as the flux equilibrates, the velocity of the discontinuity goes to zero. Similarly, the velocity of an energy discontinuity between liquid and vapor is

$$V = \frac{E_{UZ} - E_{TZ} - h_{fg} q_c}{C_{UZ} - C_{TZ}} \tag{2-56}$$

$$E = c_l q_l + c_v q_v - K \frac{\partial T}{\partial n} \tag{2-57}$$

where E represents total energy flux; UZ and TZ denote the unsaturated zone (liquid) and thermal zone (vapor), respectively; q_c is the mass flux across the interface (positive for condensation of vapor at the interface); c_l and c_v represent enthalpy per unit mass of liquid and vapor; K is the bulk thermal conductivity; h_{fg} is the enthalpy associated with phase change; and C represents total energy capacitance.

Assuming liquid is on side 2 and vapor on side 1, the velocity of the discontinuity can be represented

$$V_l = R_l (q_l - q_v) \tag{2-58}$$

$$V_v = R_v (q_c - q_v) \tag{2-59}$$

$$V_e = C_l q_l - C_v q_v - C_c q_c + \epsilon \tag{2-60}$$

$$R_l = \frac{1}{\epsilon \left(\theta_{l2} - \theta_{l1}\right)} \tag{2-61}$$

$$R_v = \frac{1}{\epsilon \left(\theta_{v2} - \theta_{v1}\right)} \tag{2-62}$$

$$C_l = \frac{c_l}{\left(C_{UZ} - C_{TZ}\right)} \tag{2-63}$$

$$C_v = \frac{c_v}{\left(C_{UZ} - C_{TZ}\right)} \tag{2-64}$$

$$C_c = \frac{h_{fg}}{\left(C_{UZ} - C_{TZ}\right)} \tag{2-65}$$

$$C_k = \frac{\left(K_{UZ}\frac{\partial T_{UZ}}{\partial n} - K_{TZ}\frac{\partial T_{TZ}}{\partial n}\right)}{\left(C_{UZ} - C_{TZ}\right)} \tag{2-66}$$

For compatibility, $V_l = V_v = V_e$.

Equating the velocities from liquid and vapor,

$$q_c = \frac{R_l q_l + R_v q_v}{R_l + R_v} \tag{2-67}$$

Equating the velocities from liquid and energy and substituting for q_c

$$q_l \left[R_l\left(R_v - C_l + C_c\right)\right] = - q_v \left[C_v\left(R_l + R_v\right) + R_v\left(C_c - R_l\right)\right] + C_k \left(R_l + R_v\right) \quad (2\text{-}68)$$

The relationship between liquid flux in the nonboiling zone and vapor flux in the boiling zone depends on the temperature gradients on both sides of the isotherm as well as the storage capacities for mass and energy.

The energy-flux balance compatibility condition is not explicitly specified. The specified-temperature condition along the isotherm is equivalent to an energy source/sink along the isotherm with the magnitude of the source determined in the solution process. The magnitude of the source is implicitly compatible with the mass fluxes through the velocity constraints.

Once the solution has been determined, the isotherm is updated using any of the expressions for velocity

$$x^{n+1} = x^n + V \Delta t \quad (2\text{-}69)$$

Note that the velocity solved for is actually the velocity magnitude in the direction normal to the isotherm.

2.6 FRACTURE GOVERNING EQUATIONS AND COMPUTATIONAL APPROACH

The same governing equations apply in the fractures as in the matrix, except that mass fluxes are fully two-phase rather than piecewise one-phase. The fracture equations are standard. Interchange between the matrix and fracture is handled through distributed sources/sinks centered on fracture elements. These sources and sinks enter into the compatibility equations for the matrix and are directly applied in the fracture equations.

There are two primary methods for handling the complete matrix/fracture system. In the direct method, the matrix equations and the fracture equations are all assembled into one large set of linearized equations, the equations are solved, the unknown values are updated, and the procedure repeats until convergence is obtained. In the iterative method, the matrix equations are solved with an initial guess for fracture conditions and the matrix conditions become known source/sink terms in the reduced fracture equations. The fracture equations are iteratively updated until close to convergence, the new set of fracture values is used in the matrix equations, and the procedure repeats until overall convergence is achieved.

The advantage of the direct method is that all unknowns are updated simultaneously, so that convergence may be improved. The disadvantage of the direct method is that the resulting matrix equations

yield a square matrix, for which the computational effort increases by $O(N^3)$, where N is the number of unknowns. Including the fracture equations into the system is not computationally attractive.

The advantage of the iterative method is that the size of the matrix arising from the boundary integral equations is minimized and the fracture equation matrix is efficient to solve. The disadvantage of the iterative method is that there is poorer linkage between matrix and fracture, which may impede convergence.

2.7 IMPLEMENTATION STATUS

An existing code with a 2D boundary integral equation module, JACQUARD, based on work by Stothoff (1991), has been obtained and enhanced to include the full set of single-potential discontinuity equations presented in section 2.3. The single potential in the equations represents temperature. JACQUARD has been tested for a series of simple heat-transfer problems, although the testing has been limited. The boundary integral formulations representing boundary conditions, line sources, material-property changes, resistant layers, and conductive fractures have all been examined for plausibility. In simple cases, exact analytic solutions have been obtained. Further testing is required before the coding can be fully reliable.

A test problem including external heat sinks along a conductive fracture, presented in section 3 in greater detail, is the strongest test of the fracture equations. The problem is a simplified representation of the refluxing problem. The boundary integral solution matches standard methods almost exactly for this problem.

Additional cursory testing based on the test problem, varying the fracture properties and the applied sources/sinks, identified problems with the original formulation for the fracture equations. The original formulation approximated jumps in potential along fractures as piecewise linear. The formulation exhibited numerical instability along the fractures, with extreme instability developing in cases that are mild compared to the situation that will be modeled at YM. The revised formulation (which is the formulation reported) approximates the jumps in potential as piecewise constant. The revised formulation is stable, even under stresses far more severe than would be anticipated in YM refluxing problems. Linking heat conduction and mass transfer in JACQUARD has been started but has not yet been completed.

16/20

3 TEST PROBLEMS

The full approach developed in section 2 has not been used before, although pieces of the boundary integral approach have been presented in various publications (Stothoff, 1991). A test problem relevant to YM includes full consideration of two-phase flow and energy transport in the fracture with heat conduction in the matrix. The conditions in the fracture in the test problem should be dependent on both the moisture fluxes imposed in the fracture and on the heating due to the repository.

In section 3.1, a simple case test is presented that captures some of the features of boiling in the fracture. The test case is used to compare the predictions of the boundary integral approach against a benchmarked finite element code currently under configuration management. The comparison is run in the predictive mode, where the temperature distribution is calculated for a prespecified sink term.

In section 3.2, the same test case is exercised in greater detail by the finite element code alone, to gain some physical insight into the effect of various infiltration scenarios on the reflux zone. Additional coding was required to perform the simulations using the boundary integral approach, precluded by time constraints; however, this comparison will be made in the near future as time permits.

3.1 CODE VERIFICATION PROBLEM

A simpler case to test significant portions of this ultimate problem, without the complications of mass transport, simulates the effect of mass transport on the energy balance with an energy sink based on the amount of latent energy bound up in boiling water. The total energy extracted by boiling water, in the form of latent heat, can be calculated as a function of the flux of water introduced at the top of the fracture. The problem is further simplified by assuming the vapor escapes the domain before condensing and releasing the energy.

Conditions representative of YM were used to compare the boundary integral formulation with simulations provided by a commercial finite element code, ABAQUS (Hibbit, Karlsson & Sorensen, Inc., 1996). The domain is 20 m wide by 100 m tall, with the sides representing symmetry conditions. The top and bottom boundary of the test case conditions were specified temperature, set arbitrarily to−50 °C and 50 °C, respectively, yielding a temperature gradient similar to that obtained from heating by WPs early in the repository performance period. Thermal conductivity was set to 2-1 W/m. One side of the domain was designated a fracture. A uniform sink of 2.4 J/m^2 was applied to the fracture side in the ABAQUS simulation while the uniform sink was applied within the fracture in the boundary integral simulation. The sink had the total strength commensurate with boiling a surface infiltration of 100 mm/yr focused over 100 m into the fracture, divided by the length of the fracture. For comparison, the fracture was assigned the same conductivity as the matrix in the boundary integral simulation. The boundary integral simulation used a domain 40 m wide rather than 20 m, with the fracture centered in the domain; this tests the formulation better without changing the numerical results.

The code predictions of temperature were compared along all boundaries and selected horizontal and vertical traverses. A comparison between the predictions of the two codes is shown in figure 3-1. In figure 3-1a, the temperatures produced by the two codes are shown for horizontal traverses 1/4, 1/2, and 3/4 of the way from the bottom to the top. In figure 3-1b, the temperatures produced by the two codes are shown along the fracture. All traverses are along nodes in the finite-element mesh. As can be seen, the two codes produce essentially identical results.

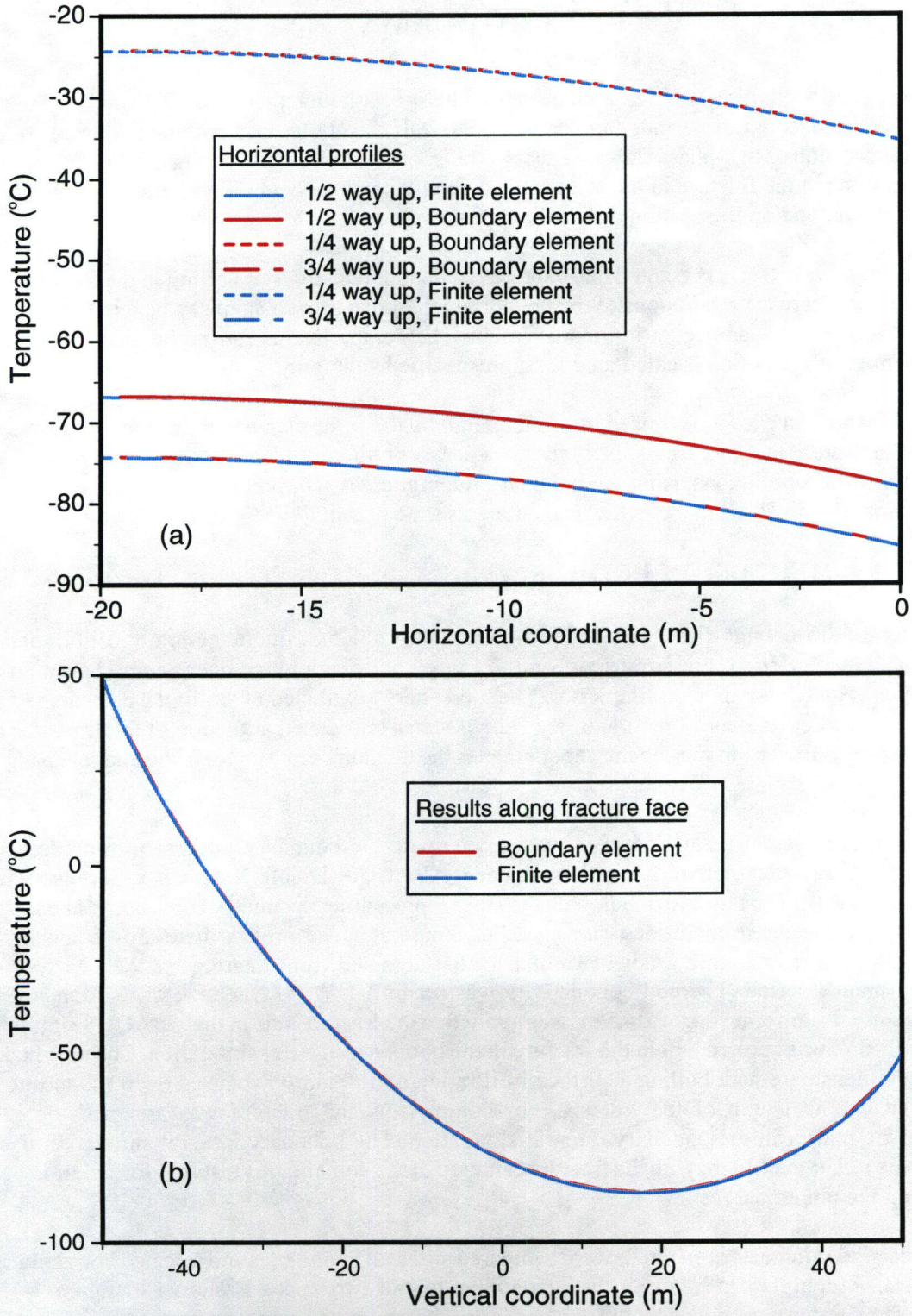

Figure 3-1. Temperature produced by ABAQUS and the boundary integral code: (a) along horizontal traverses located 1/4, 1/2, and 3/4 of the way from the bottom to the top of the domain, and (b) along the fracture wall

3.2 FINITE ELEMENT ANALYSES OF THE EFFECTS OF FRACTURE-WALL EVAPORATION AND CONDENSATION ON TEMPERATURE

Steady-state heat conduction analyses were performed, with fracture-wall evaporation and condensation simulated as heat sinks and sources, to examine the effects of fracture-driven water on temperatures in the surrounding rock. Fracture water may affect rock temperature through (i) the cooling effect of water flowing down from cooler areas of the rock, (ii) extraction of latent heat from the evaporation zone, and (iii) release of latent heat in the condensation zone (figure 3-2). The cooling effect of liquid water was not included in the current analyses but will be considered in subsequent analyses (section 2). The effects of evaporation and condensation were accounted for through a heat sink q_e and source q_c applied on the fracture wall in the evaporation and condensation zones, respectively.

The fracture-wall evaporation zone consists of the area of the fracture above the heat source for which temperature, T (°C), lies in the range $95 \le T \le 105$. Similarly, the fracture-wall condensation zone is the area of the fracture below the heat source for which $T<95$. The locations and extent of both zones depend on the solution from the heat conduction analysis. As a result, each analysis consisted of a series of iterations in which the locations and extent of the evaporation and condensation zones were adjusted to obtain consistent values between successive iterations.

The heat sink q_e and source q_c were evaluated as follows:

$$q_e = -\rho_w v_w h_c / 2A_c \tag{3-1}$$

$$q_c = \rho_w v_w h_c / 2A_c \tag{3-2}$$

where ρ_w and h_c are the density and latent heat of water, respectively, which are currently set to constant values of 1,000 kg/m^3 and 2.26×10^6 J/kg, respectively, but will be specified as functions of temperature in subsequent analyses; A_e and A_c are the areas (m^2/m) of the evaporation and condensation zones, respectively; and V_w is the instantaneous volume of water supplied by net infiltration. The factor of ½ in Eqs. (3-1) and (3-2) arises from the fact that only one side of the fracture was modeled (i.e., fracture was treated as a vertical symmetry plane). V_w was evaluated using

$$V_w = w_{in} L_{fc} (\Delta t) \tag{3-3}$$

in which w_{in} is the net infiltration rate (m/s), L_{fc} is the fracture catchment area, at times referred to as funnel factor (m^2/m), and Δt (= 1 s) is length of time over which the infiltration rate was integrated to obtain a time-independent value for V_w. The parameter L_{fc} was set to 100 m (but will be varied in subsequent analyses), w_{in} was varied between analysis cases, and both A_e and A_c were varied iteratively within each analysis as described previously.

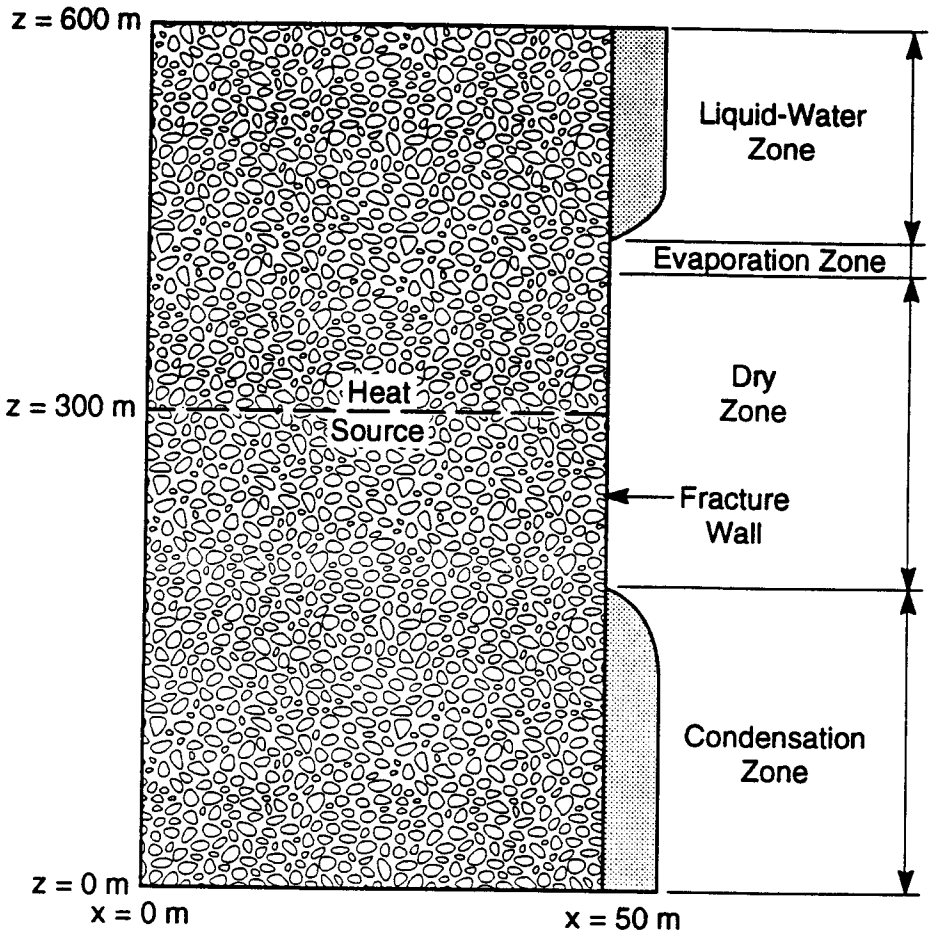

Figure 3-2. Problem geometry showing boundary conditions and location of applied heat source

3.2.1 Model Description

The model domain consists of a rectangular strip of rock 50 m ($= L_{fc}/2$) wide by 600 m high (figure 3-2). The fracture wall is represented by the right-side boundary (x = 50 m), at which a normal flux q (J/m^2) was applied; $q = q_c$ in the evaporation zone, $q = q_c$ in the condensation zone, and $q = 0$ elsewhere on the fracture wall because of symmetry. Zero normal flux was also applied on the left-side boundary (x = 0). Constant temperature of magnitude 15 °C and 27 °C was applied on the top and bottom boundaries, respectively. A constant surface heat source q_s (J/m^2) was applied over the full width of the model at mid depth (z = 300 m). Analyses were performed for two values of q_s, 0.725 and 1.08 J/m^2, which were selected to give maximum temperatures of 125 °C and 175 °C, respectively, under zero net infiltration. The analyses were performed using ABAQUS Version 5.6, (Hibbit, Karlsson & Sorensen, Inc., 1996).

18/20

3.2.2 Results

Results of the finite-element analyses (table 3-1 and figure 3-3) indicate that fracture-driven liquid water may break through the heat-source horizon depending on the strength of the heat source and net infiltration rate. For a source strength of 0.725 J/m^2, which would give a maximum temperature of 125 °C

Table 3-1. Results of finite element analyses, showing locations of the boiling isotherm for various infiltration rates and heat source strength

Analysis Cases	Source Strength (J/m^2)	Net Infiltration (mm/yr)	Relative Elevation of 100 °C Isotherm	
			z_h-z_{lower} (m)	z_{upper}-z_h (m)
1	0.725	1	74	56
2	0.725	10	T_{wmax}<100 °C	T_{wmax}<100 °C
3	0.725	5	49	16
4	1.08	5	153	101
5	1.08	10	153	54
6	1.08	20	T_{wmax}<100 °C	T_{wmax}<100 °C
z_h, z_{lower}, and z_{upper} are the z-coordinates (figure 3-1) of the heat source and lower and upper 100 °C isotherms, respectively; T_{wmax} is maximum fracture-wall temperature				

under zero net infiltration, the minimum infiltration rate that would cause fracture water to contact the heat source lies between 1 and 10 mm/yr. The break-through infiltration lies between 10 and 20 mm/yr for a higher heat source of 1.08 J/m^2, which would give a maximum temperature of 175 °C under zero net infiltration. The value of the fracture catchment area L_{fc}, which was held constant at 100 m^2/m for these analyses, is expected to affect the relationship between break-through infiltration and source strength, because the available water volume V_w is directly proportional to L_{fc}.

These results indicate that the approach of simulating condensation and evaporation as heat sources and sinks in a heat conduction analysis can be successfully applied to determine relationships between heat source strength and break-through infiltration. Further refinement of the model is required to assign more meaning to the results. Other processes that may also affect the fracture-wall temperature include exchange of liquid water and vapor between fracture and rock matrix, condensation above the upper boiling isotherm, and liquid-phase advection.

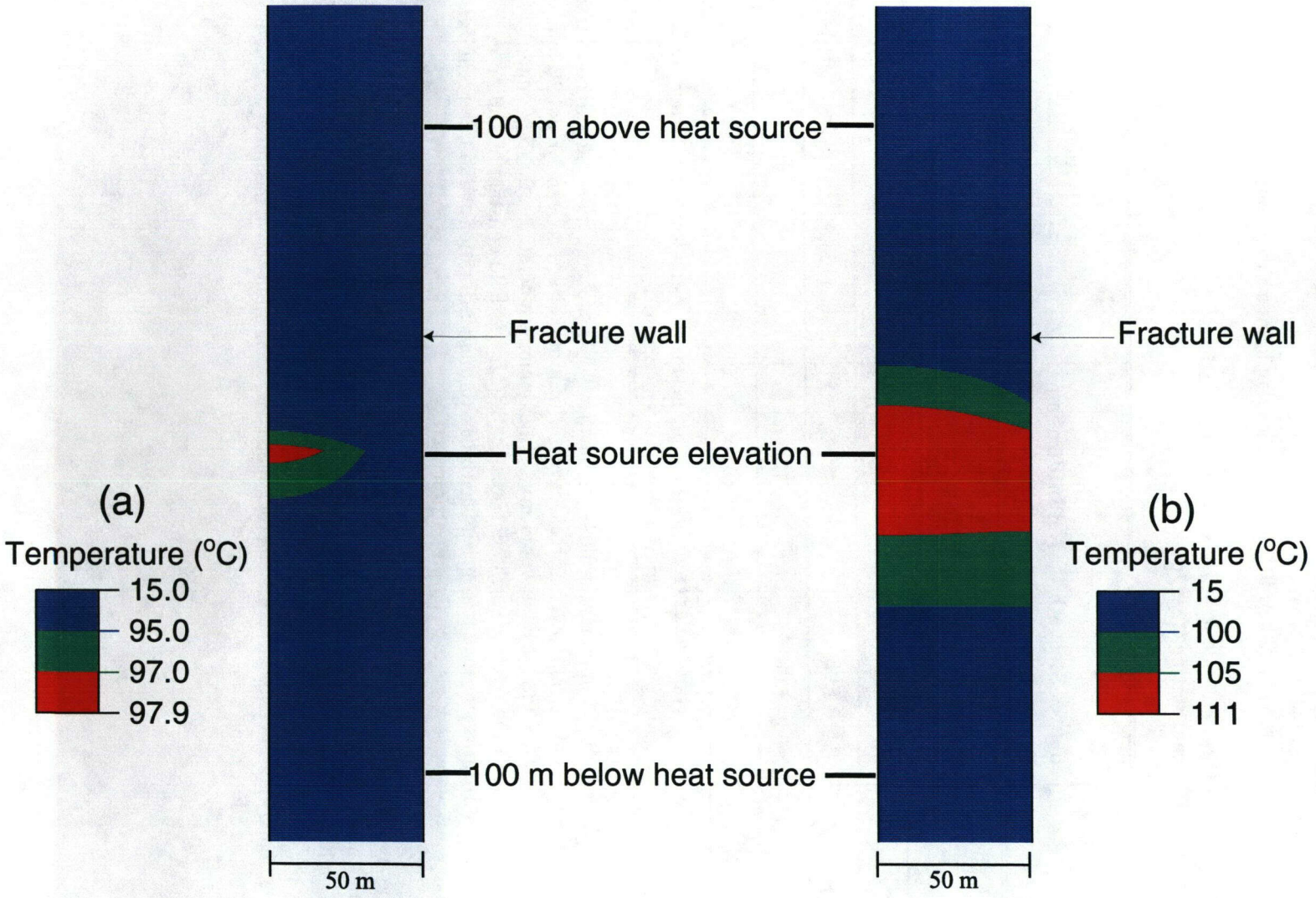

Figure 3-3. Temperature distributions for (a) case 2, for which temperature is below boiling everywhere, and (b) case 3, for which above-boiling conditions occur (table 3-1)

4 SUMMARY

This report documents work performed by the CNWRA toward quantifying the durations and magnitudes of water fluxes contacting WPs during the thermally perturbed period subsequent to emplacement of the WPs. Evidence of water contacting heaters has been reported in the literature for several experiments conducted in fractured porous media, so that it is indisputable that thermally mobilized water can drip onto WPs. The duration and magnitude of such fluxes cannot be ascertained from the limited spatial and temporal scales of the experiments and it is difficult to project the results into cases where different ambient water fluxes occur. Accordingly, quantification of water fluxes must resort to numerical experimentation.

Simulations at the drift scale are awkward to perform, as there are too many fractures for realistic discrete-fracture simulations and too few fractures for representative continuum simulations. In addition, the disparate spatial and temporal scales between matrix and fracture yield extremely computationally burdensome simulations. These difficulties have been recognized for years by the CNWRA and the NRC. To ease some of the computational burden, an innovative approach is being examined that only discretizes on the boundaries and fractures, using boundary integral techniques to treat heat and mass balances within the rock matrix and standard numerical approaches to handle the fractures. The theoretical basis and early test results indicate the boundary integral approach and standard methods provide comparable predictions.

The test problem is relevant to conditions at YM, although only the energy balance is considered; the details of mass transfer are neglected. Simulations using the test problem (solved using standard numerical techniques) with heat-source rates corresponding to different periods after emplacement, suggest that dripping may not be precluded with plausible infiltration rates and focusing conditions, even when thermal fluxes are at a maximum. Vapor transport, which is an alternative pathway for infiltrating water to pass through the repository horizon, is not included in the analysis and may limit the dripping fluxes.

5 REFERENCES

Bird, R.B., W.E. Stewart, and E.N. Lightfoot. 1960. *Transport Phenomena.* New York: John Wiley & Sons.

Buscheck, T.A., J.J. Nitao, and D.G. Wilder. 1993. Repository-heat-driven hydrothermal flow at Yucca Mountain, Part 2: Large-scale *in situ* heater tests. *Nuclear Technology* 104: 418–448.

Buscheck, T.A., and J.J. Nitao. 1995. *Thermal-Hydrological analysis of large-scale thermal tests in the exploratory studies facility at Yucca Mountain.* UCRL–ID–121791. Livermore, CA: Lawrence Livermore National Laboratory.

Gardner, W.R. 1958. Some steady state solutions of the unsaturated moisture flow equation with application to evaporation from a water table. *Soil Science* 85: 228–232.

Hibbit, Karlsson, & Sorensen, Inc. 1996. *ABAQUS User's Manual Version 5.6.* Pawtucket, RI: Hibbit, Karlsson, and Sorensen, Inc.

Ingber, M.S., and A.K. Mitra. 1989. The evaluation of the normal derivative along the boundary in the direct boundary element method. *Applied Mathematical Modelling* 13: 32–40.

Lichtner, P.C., and M.S. Seth. 1998. *MULTIFLO Users Manual: MULTIFLO Version 1.2β Two-Phase Nonisothermal Coupled Thermal-Hydrologic-Chemical Flow Simulator.* San Antonio, TX: Center for Nuclear Waste Regulatory Analyses.

Liggett, J.A., and P.L-F. Liu. 1983. *The Boundary Integral Equation Method for Porous Media Flow.* London, England: George Allen & Unwin.

Patrick, W.C. 1986. *Spent Fuel Test—Climax: An Evaluation of the Technical Feasibility of Geologic Storage of Spent Nuclear Fuel in Granite.* Final Report. UCRL–553702. Lawrence, CA: Lawrence Livermore National Laboratory.

Pullan, A.J., and I.F. Collins. 1987. Two- and three-dimensional steady quasi-linear infiltration from buried and surface cavities using boundary element techniques. *Water Resources Research 23*(8): 1,633–1,644.

Ramirez, A.L. 1991. *Prototype Barrier System Field Test (PEBSFT).* Final Report. UCRL–ID–106159. Lawrence, CA: Lawrence Livermore National Laboratory.

Stothoff, S.A. 1991. *A Boundary integral technique for modelling two-phase flow in porous media.* PhD. Dissertation. Princeton University.